NISSUNA UMANA INVESTIGAZIONE SI PUO DIMANDARE VERA SCIENZIA
S'ESSA NON PASSA PER LE MATEMATICHE DIMOSTRAZIONI
LEONARDO DA VINCI

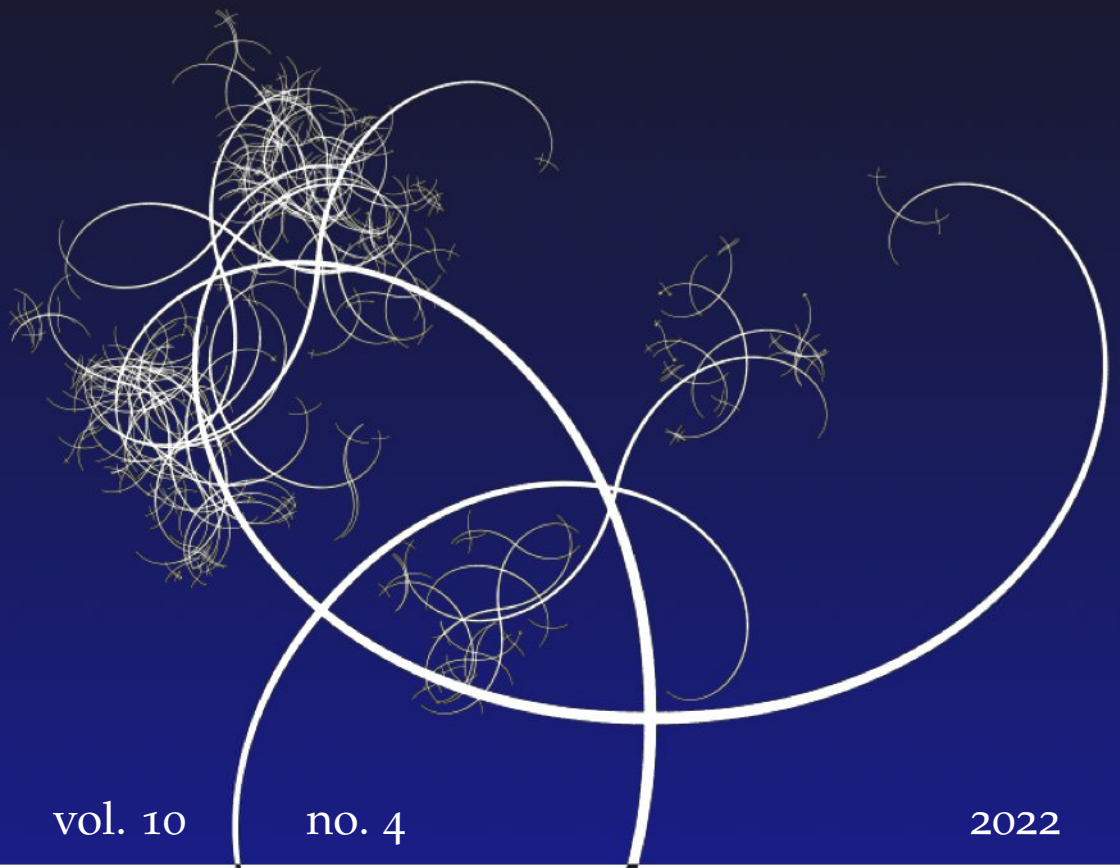

vol. 10 no. 4 2022

Mathematics and Mechanics *of* Complex Systems

Roy Burson and Koffi Enakoutsa

DUCTILE VOID GROWING IN MICROMORPHIC GLPD POROUS PLASTIC SOLIDS CONTAINING TWO POPULATIONS OF CAVITIES WITH DIFFERENT SIZES

msp

MATHEMATICS AND MECHANICS OF COMPLEX SYSTEMS
Vol. 10, No. 4, 2022
https://doi.org/10.2140/memocs.2022.10.395

DUCTILE VOID GROWING IN MICROMORPHIC GLPD POROUS PLASTIC SOLIDS CONTAINING TWO POPULATIONS OF CAVITIES WITH DIFFERENT SIZES

ROY BURSON AND KOFFI ENAKOUTSA

Gologanu, Leblond, Perrin, and Devaux (GLPD) developed a constitutive model for ductile fracture for porous metals based on generalized continuum mechanics assumptions. The model predicted with high accuracy ductile fracture process in porous metals subjected to several complex loads. The GLDP model performances over its competitors has attracted the attention of several authors who explored additional capabilities of the model. This paper provides analytical solutions for the problem of a porous hollow sphere subjected to hydrostatic loadings, the matrix of the hollow sphere obeying the GLPD model. The exact solution for the expressions of the stress and the generalized stress the GLPD model involved are illustrated for the case where the matrix material does not contain any voids. The results show that the singularities obtained in the stress distribution with the local Gurson model are smoothed out, as expected with any generalized continuum model. The paper also presents some elements of the analytical solution for the case where the matrix is porous and obeys the full GLPD model at the initial time when the porosity is fixed. The later analytical solution can serve to predict the mechanisms of ductile fracture in porous ductile solids with two populations of cavities with different sizes.

1. Introduction

Metal structures often fail by ductile rupture when they are subjected to external static or dynamic forces. The need to develop physical, mechanical and mathematical constitutive models to precisely predict ductile fracture processes in metals is acutely felt in the metal structure design community. So far, the community has widely accepted that the model proposed [18] and extended in [28; 29] to account for cavity interactions and coalescence following an earlier suggestion in [26] can adequately describe ductile fracture in metals. Several extensions have followed these pioneering works; among them, let us mention the contributions [21; 22], and recently [20]. The latter has modified Gurson model to include shear failure which often occurs, for instance, during high velocity impact failures of many steels.

Communicated by Francesco dell'Isola.
MSC2020: 74A45, 74C05.
Keywords: gradient model, analytical solution, plasticity, hollow sphere problem, fracture.

Another modification of Gurson model including a characteristic length scale aimed at eliminating the pathological post-bifurcation mesh dependence issues proposed in [19] based on a previous suggestion of [23] in the context of concrete damage was adopted in [30; 31]. This proposal was studied in detail in [7; 13] and adopted (thanks to its successes) in the context of high rate deformation and failure of materials in [1; 14; 15]. However, the proposal was less satisfactory from the theoretical and physical viewpoints since it does not rely on any serious physical justification. This was the motivation of the development by Gologanu, Leblond, Perrin, and Devaux [17] of a second-gradient micromorphic model[1] for porous plastic materials. The GLPD model was obtained from a refinement of [2]'s original homogenization procedure, which was based on conditions of homogeneous boundary strain rate.

In contrast, the boundary velocity in the GLPD model approach was assumed to be a quadratic, rather than linear, function of the coordinates. The physical idea behind this assumption was to account in this way for possible quick variations of the macroscopic strain rate over very short distances, for example at the scale of the elementary cell the GLPD model is based on. The output of the procedure was a model of "micromorphic" nature, involving the second gradient of the macroscopic velocity and generalized macroscopic stresses of "moment" type (homogeneous to the product of a stress and a distance.) Other type of higher-order gradient models involving third-rank stress tensor with applications in bone remodeling design and other domain of interest exist. Among them let us mention the works [27; 16; 6].

In practice, the GLPD model was extensively studied in [7; 11], where it was notably shown that the model has the ability to predict mesh-independent FE solutions and to reproduce satisfactorily ductile fracture tests. Other numerical simulations involving second gradient models are available in the literature; see for instance [3; 24; 25]. A recent modification of the GLPD model numerical implementation developed in [7; 11] was suggested in [4] and yielded the same conclusions. The assessment of the reliability and accuracy of these two algorithms requires the development of analytical solutions that have served as critical cross references, see [7; 9; 10]. These solutions are based on two crude approximations so as for analytical solutions to be amenable: the porosity in the matrix material of the geometry considered was assumed to vanish.

The objective of the present paper is twofold: (i) follow up the study of applications of the GLPD model to simple problems that might be of interest to validate the numerical implementation of this model into a finite element code and (ii) use the mechanical fields found to model cracking mechanisms in porous ductile solids containing two populations of cavities. The problem considered here is

[1]We refer to micromorphic models as GLPD models for short.

a hollow sphere subjected to a hydrostatic tension and made of a porous plastic material, obeying the GLPD model. We found the analytic solution of the hollow sphere problem in terms of deformation, stress and moment distributions under the conditions that the matrix obeys a reduced GLPD model for the case where the porosity vanishes. Also, we consider some elements of the solution of the problem in the presence of porosity in the matrix material, which is a rather complex type of problem. The complexity of the latter problem (a highly nonlinear problem) forces us to present only some elements of the analytical solution at the initial time when the porosity is held constant. The rest of the paper is structured as follows:

- Section 2 describes the problem model, a hollow sphere subjected to an hydrostatic loading, the matrix obeying the GLPD model.
- In Section 3 we assess the solution obtained for the case where the porosity vanishes. An algorithm that simulates the behavior of this model and analyzes the effects of the characteristic length scale on the distribution of stress and moments is also presented.
- Section 4 considers the solution of the problem for the case where the porosity does not vanish at the initial time. We provide implicit analytic expressions for the Cauchy stress and moment components based on a highly nonlinear ordinary differential equation, which involves the length scale of the GLPD model. Using then the associated flow rule we calculate the radial velocity. Employing the evolution law for the porosity we then derive the growth rate of the voids located in the matrix.
- The concluding Section 5 discusses the results of our analytical solutions with and without porosity.

2. Presentation of the hollow porous sphere problem

We consider a hollow sphere of inner radius a_0 and outer radius b_0, representing an elementary cell of a porous plastic metal; see Figure 1. The matrix contains

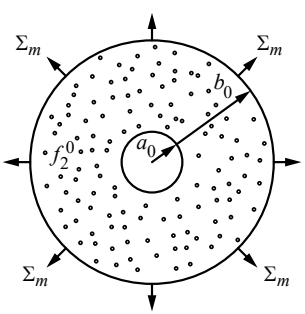

Figure 1. The hollow sphere model problem being considered.

secondary small, dispersed voids; its porosity (void volume fraction) is initially uniform and denoted f_2^0. The boundary of the central void is free of traction whereas the outer boundary is subjected to some overall hydrostatic tension $\boldsymbol{\Sigma}_m$. The details of the derivation of these boundary conditions can be found in Appendix B. The matrix material of the porous hollow sphere is supposed to obey the GLPD constitutive model as described in Appendix A and in [17]. The hollow sphere model problem presented here have served to find the solutions of several ductile fracture problems the solution of which have yields micromechanics based models for ductile porous metals under various loading conditions. Some of these problems, with their solutions, can be found in [7; 9; 21; 22].

3. Analytical solution when porosity is neglected

3.1. ***Derivation of the mechanical fields.*** We seek a solution of the spherical shell problem for purely ideal-plastic behavior, the yield stress in simple tension being denoted by Σ_0 and the porosity in the matrix being neglected. As a result, the yield criterion (45) reduces to

$$\Phi(\boldsymbol{\Sigma}, \boldsymbol{M}, \Sigma) \equiv \frac{1}{\Sigma^2}\left(\Sigma_{\text{eq}}^2 + \frac{Q^2}{b^2}\right) - 1 = 0. \tag{1}$$

In this equation:

- $\boldsymbol{\Sigma}$ represents the ordinary second-rank symmetric Cauchy stress tensor and $\boldsymbol{M}$ is the third-rank moment tensor, symmetric in its first two indices only. The components of $\boldsymbol{M}$ satisfy
$$M_{ijj} = 0. \tag{2}$$
- $\Sigma_{\text{eq}} \equiv \left(\frac{3}{2}\boldsymbol{\Sigma}' : \boldsymbol{\Sigma}'\right)^{\frac{1}{2}}$ is the von Mises equivalent stress, $\boldsymbol{\Sigma}'$ being the deviator of $\boldsymbol{\Sigma}$.
- Σ represents a kind of average yield stress in the heterogeneous metallic matrix.
- Q^2 is a quadratic form of the components of the moment tensor given by
$$Q^2 \equiv A_1\mathcal{M}_1 + A_2\mathcal{M}_2, \quad \text{with } A_1 = 0.194,\ A_2 = 6.108, \tag{3}$$
where
$$\mathcal{M}_1 \equiv M_{mk}M_{mk}, \quad \mathcal{M}_2 \equiv \tfrac{3}{2}M'_{ijk}M'_{ijk}, \tag{4}$$
are the quadratic invariants of $\boldsymbol{M}$; here $M_{mk} \equiv \frac{1}{3}M_{hhk}$ and $\boldsymbol{M}'$ denote the mean and deviatoric parts of $\boldsymbol{M}$, taken over its first two indices.
- b represents the characteristic length scale.

After development, the flow rule (47) becomes (see [7; 11] for details)

$$\dot{D}^p_{ij} = \eta\frac{3}{\Sigma_0^2}\Sigma'_{ij}, \quad (\nabla\dot{D})^p_{ijk} = \frac{\eta}{{\Sigma_0}^2 b^2}\left(\tfrac{2}{3}A_I\delta_{ij}M_{mk} + 3A_{II}M'_{ijk}\right) + \delta_{ik}U_j + \delta_{jk}U_i,$$

where $M_{mk}\frac{1}{3}M_{hhk}$ and $\boldsymbol{M}'$ are as above and η is the plastic multiplier, determined from the consistency condition and satisfying

$$\eta \begin{cases} = 0 & \text{if } \Phi(\boldsymbol{\Sigma}, \boldsymbol{M}, \Sigma) < 0, \\ \geq 0 & \text{if } \Phi(\boldsymbol{\Sigma}, \boldsymbol{M}, \Sigma) = 0. \end{cases}$$

We shall also assume that the parameter A_I vanishes for the analytical solution to be amenable. Another, subtler reason for this choice is that the value of A_I in the GLPD model, 0.194, is much smaller than that of A_{II}, 6.108; hence, the value of A_I can safely be neglected. The remaining equations of the GLPD constitutive relations for ductile porous materials can be found in Appendix A and in [17].

We are looking for a solution in which the spherical shell is entirely plastic, so that the yield function $\Phi(\boldsymbol{\Sigma}, \boldsymbol{M}, \Sigma_0)$ is zero everywhere. We briefly review the solution procedure given in [8]. Consider the velocity, strain rate and its gradient fields first. As in the case of purely elastic behavior, the matrix of spherical shell is incompressible; as a result, the velocity field is radial and given by

$$\mathcal{U} = \frac{A}{r^2}, \tag{5}$$

where A is a parameter independent of the material point position r.

Using the flow rule and the incompressibility of the material, the nonzero components of the stress and moment fields are found to be

$$\Sigma'_{rr} = -\frac{1}{\eta}\frac{2A\Sigma_0^2}{3r^2}, \qquad \Sigma'_{\theta\theta} = \Sigma'_{\phi\phi} = \frac{1}{\eta}\frac{A\Sigma_0^2}{3r^2}, \tag{6}$$

$$M'_{rrr} = \frac{1}{\eta}\frac{2A\Sigma_0^2 b^2}{A_{II}r^4}, \quad M_{r\theta\theta} = M_{r\phi\phi} = -\frac{1}{\eta}\frac{A\Sigma_0^2 b^2}{A_{II}r^4}, \tag{7}$$

$$M'_{\theta\theta r} = M'_{\phi\phi r} = -\frac{1}{\eta}\frac{A\Sigma_0^2 b^2}{A_{II}r^4}. \tag{8}$$

The conditions $M_{ijj} = 0$ and the expressions of M'_{rrr} and $M_{r\theta\theta}$ in (8) yield

$$M_{rrr} = -2M_{r\theta\theta}, \quad M_{\theta\theta r} = M'_{\theta\theta r}.$$

Substituting the formulas for stress and moment, (6)–(8), in the reduced yield criterion (1), we get the following expression for the plastic multiplier η:

$$\eta = \frac{A\Sigma_0}{r^3}\sqrt{1 + \frac{15}{A_{II}}\frac{b^2}{r^2}}. \tag{9}$$

This completes the specification of the nonzero components of the moment tensor. However, the full expressions of the nonzero components of the ordinary stress tensor are still unknown. After a tedious but straightforward calculation using the expressions of the nonzero components of the moment tensor, the spherical

symmetry properties of the problem, and the fact that $\Sigma_{rr} - \Sigma_{\theta\theta} = \Sigma'_{rr} - \Sigma'_{\theta\theta}$, the formulas for the nonzero components of the ordinary Cauchy stress tensor are obtained as

$$\frac{d\Sigma_{rr}}{dr} = f(r) \tag{10}$$

with

$$f(r) = \frac{2A\Sigma_0^2}{\eta r^3} + \frac{2(\eta''\eta^2 - 2\eta'^2\eta)}{\eta^4}\frac{A\Sigma_0^2 b^2}{A_{II} r^4} - \frac{28\eta'}{\eta^2}\frac{A\Sigma_0^2 b^2}{A_{II} r^5} - \left(\frac{72}{\eta} + \frac{2\eta'}{\eta^2}\right)\frac{A\Sigma_0^2 b^2}{A_{II} r^6} - \frac{8A\Sigma_0^2 b^2}{\eta A_{II} r^7}, \tag{11}$$

the primes denoting differentiation with respect to r. Equation (10) implicitly defines the expression of the component Σ_{rr} of the stress tensor. The nonzero components of the stress tensor are obtained as

$$\Sigma_{rr} = \int_{r_i}^{r} f(\tau)d\tau, \quad \Sigma_{\theta\theta} = \Sigma_{\phi\phi} = \Sigma_{rr} - \frac{1}{\eta}\frac{A\Sigma_0^2}{r^2}. \tag{12}$$

The solution of (12) along with the nonzero components of the moment provided above automatically satisfy the balance equations.

3.2. ***Numerical illustrations of the solution.*** We now illustrate the analytic solution presented in [8], both graphically and by giving explicit expressions for the stress and moment tensors. We do so by evaluating the integral equation (12) using a FORTRAN routine we developed. Each integral has also been evaluated analytically so that we possess the exact solution. We use the following material and model parameters:

internal radius $r_i = 0.05$ m
yield stress $\Sigma_0 = 100$ MPa
parameters: $A = 0.001$ m, $A_1 = 0.194$, $A_2 = 6.108$

Figure 2 plots the solutions for the stress components Σ_{rr}, $\Sigma_{\theta\theta}$, and the moment component M_{rrr}, using the analytical expressions of these components of the Cauchy stress and the moment tensor obtained in [8]. The figure shows that singularities are absent from the stress, and there is no discontinuity near the void as the Gurson model would have predicted.

4. Analytical solution in the presence of porosity in the matrix

In this section we present the solution to the hollow sphere problem for the case where the matrix obeys the full GLPD model. Therefore, we loose the simplification

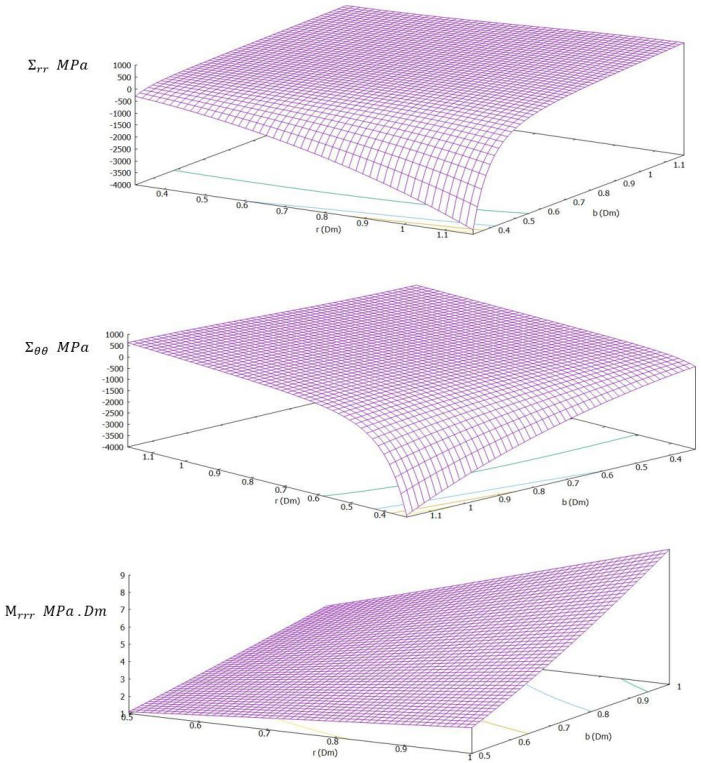

Figure 2. Graphs of the stress components Σ_{rr}, $\Sigma_{\theta\theta}$ and the moment component M_{rrr} versus the radial coordinate r and the characteristic length scale b. The surfaces obtained are all smooth; the singularity in the Cauchy stress obtained with the first gradient model has been smoothed out with second gradient model effects.

that yields the prior results [8]. A detailed derivation of the solution is presented in Burson and Enakoutsa [5]; only highlights are given here.

4.1. ***Derivation of Cauchy stress components.*** The setup of the problem, taken from [8], consists of the balance equation

$$\frac{d\Sigma_{rr}}{dr}+\frac{2}{r}(\Sigma_{rr}-\Sigma_{\theta\theta})-\frac{d^2M_{rrr}}{dr^2}-\frac{4}{r}\frac{dM_{rrr}}{dr}-\frac{2}{r^2}M_{rrr} +\frac{2}{r^2}\frac{dM_{\theta\theta r}}{dr}+\frac{4}{r}\frac{dM_{r\theta\theta}}{dr}+\frac{8}{r^2}M_{r\theta\theta}=0, \quad (13)$$

the yield criterion

$$\frac{1}{\Sigma^2}\left(\Sigma_{\text{eq}}^2+\frac{Q^2}{b^2}\right)+2p\cosh\left(\frac{3}{2}\frac{\Sigma_m}{\Sigma}\right)-1-p^2=0, \quad (14)$$

and the boundary conditions

$$r^2\Sigma_{rr} - \frac{d}{dr}(r^2 M_{rrr}) + 4r M_{r\theta\theta} = 0, \quad M_{rrr} = 0,$$

for $r = r_i$ and $r = r_e$. Here M_{rrr} and $M_{r\theta\theta}$ are the components of the moment tensor $\boldsymbol{M}$, Σ_{rr} and $\Sigma_{\theta\theta}$ are the nonzero components of the stress tensor $\boldsymbol{\Sigma}$, Σ_m is the mean stress, and Σ_{eq} is the von Mises stress.

The stress components Σ_{rr} and $\Sigma_{\theta\theta}$ in the balance equation (13) can be expressed in terms of the invariants Σ_m and Σ_{eq} as follows:

$$\frac{d\Sigma_{rr}}{dr} + \frac{2}{r}(\Sigma_{rr} - \Sigma_{\theta\theta}) = \frac{2}{3\sqrt{3}}\frac{d}{dr}\Sigma_{\text{eq}} + \frac{2}{r\sqrt{3}}\Sigma_{\text{eq}} + \frac{d}{dr}\Sigma_m. \tag{15}$$

We have for Σ_{eq} see [5] the differential equation

$$\frac{d}{dr}\Sigma_{\text{eq}} = \frac{\alpha\left(\Sigma_0 - \Sigma_{\text{eq}}^2\right) - \frac{6}{r}\Sigma_{\text{eq}}\left(\Sigma_0 - \Sigma_{\text{eq}}^2\right)^{1/2} + \lambda}{\left(\Sigma_0 - \Sigma_{\text{eq}}^2\right)^{1/2} - \beta\Sigma_{\text{eq}}}. \tag{16}$$

Its solution for Σ_{eq} also furnishes Σ_m, which leads to Σ_{rr} and Σ_θ via the linear system

$$\begin{pmatrix}\Sigma_{\text{eq}}\\ \Sigma_m\end{pmatrix} = \begin{pmatrix}\sqrt{3} & -\sqrt{3}\\ 1 & 2\end{pmatrix}\begin{pmatrix}\Sigma_{rr}\\ \Sigma_{\theta\theta}\end{pmatrix}, \tag{17}$$

namely

$$\Sigma_{rr} = \frac{2}{3\sqrt{3}}\Sigma_{\text{eq}} + \frac{1}{3}\Sigma_m, \quad \Sigma_{\theta\theta} = \frac{1}{3}\Sigma_m - \frac{1}{3\sqrt{3}}\Sigma_{\text{eq}}. \tag{18}$$

4.2. ***Derivation of the moment tensor components.*** We now derive the components of the moment tensor $\boldsymbol{M}$. The moment components M_{ijk} are recovered by the use of the flow rule and the velocity field, which we assume can be represented as

$$\mathcal{U} = (f(r), 0, 0)$$

for some function $f(r)$ depending on the radial coordinate r. With this assumption the GLPD flow rule reduces to

$$\nabla D_{mk} = \tfrac{2}{3}\eta U_k,$$

where η is the plastic multiplier and U the velocity field (see [8] for details). In accordance with [8, eq. (36)], when $A_1 = 0$ the strain rate components are

$$\begin{aligned}
(\nabla D)_{rrr} &= \frac{df}{dr} = \frac{\eta}{\Sigma_0^2 b^2} 3A_2 M'_{rrr}, \qquad (\nabla D)_{r\theta\theta} = 0 = \frac{\eta}{\Sigma_0^2 b^2} 3A_2 M'_{\theta\theta r},\\
(\nabla D)_{\theta\theta r} &= \frac{1}{r}\frac{df}{dr} = \frac{\eta}{\Sigma_0^2 b^2} 3A_2 M'_{r\theta\theta}, \quad (\nabla D)_{r\phi\phi} = \frac{1}{r}\frac{df}{dr} = \frac{\eta}{\Sigma_0^2 b^2} 3A_2 M_{r\theta\theta}.
\end{aligned} \tag{19}$$

Let

$$\kappa = \frac{\Sigma_0^2 b^2}{3A_2}. \tag{20}$$

The deviatoric parts of the moment $\boldsymbol{M}$ satisfy

$$M'_{rrr} = \frac{\kappa}{\eta}\frac{df}{dr}, \quad M'_{\theta\theta r} = 0, \quad M'_{r\theta\theta} = \frac{\kappa}{\eta}\frac{1}{r}\frac{df}{dr}, \quad M_{r\theta\theta} = \frac{\kappa}{\eta}\frac{1}{r}\frac{df}{dr}.$$

The value of Q^2 is then computed as

$$Q^2 = \frac{3}{2}A_2\left(\frac{df}{dr}\frac{\kappa}{\eta}\right)^2\left(\frac{r^2+1}{r^2}\right).$$

Using the yield criterion we find that f satisfies the differential equation

$$\left(\frac{df}{dr}\right)^2 = \frac{2}{3A_2}\left(\frac{\eta}{\kappa}\right)^2\left(\frac{r^2}{r^2+1}\right)b^2\left(\Sigma^2\left(p^2+1-2p\cosh\left(\frac{3}{2}\frac{\Sigma_m}{\Sigma}\right)\right)-\Sigma_{\text{eq}}^2\right).$$

Using [8, (37)] we get the deviatoric part of the stress

$$\Sigma'_{rr} = -\frac{\Sigma_0^2}{3}\frac{1}{\eta}f(r), \quad \Sigma'_{\theta\theta} = \frac{\Sigma_0^2}{3}\frac{1}{\eta}f(r). \tag{21}$$

and from there the plastic multiplier satisfies

$$\eta = \tfrac{1}{2}\Sigma_0^2 f(r)\Big/\left(\Sigma_m - \frac{1}{\sqrt{3}\Sigma_{\text{eq}}}\right), \tag{22}$$

where Σ_m and Σ_{eq} are as in the previous section. Substituting (22) into (21) yields

$$\left(\frac{df}{dr}\right)^2 = f(r)^2 p(r), \tag{23}$$

where $p(r) = h(r)\iota(r)j(r)$, with

$$\iota(r) = \frac{\Sigma_0^4}{6(\Sigma_m - \frac{1}{\sqrt{3}\Sigma_{\text{eq}}})^2\kappa^2 A_2}, \quad j(r) = \frac{r^2}{r^2+1},$$
$$h(r) = b^2\left(\Sigma^2\left(p^2+1-2p\cosh\left(\frac{3}{2}\frac{\Sigma_m}{\Sigma}\right)\right)-\Sigma_{\text{eq}}^2\right).$$

Next, the nonzero components of the moment are recovered from (19) as

$$M'_{rrr} = \frac{\kappa}{\eta}\frac{df}{dr}, \quad M'_{\theta\theta r} = M'_{\phi\phi r} = \frac{-\kappa}{\eta}\frac{1}{r}\frac{df}{dr}, \quad M'_{r\theta\theta} = M_{r\theta\theta} = \frac{\kappa}{\eta}\frac{1}{r}\frac{df}{dr}, \tag{25}$$

where η and κ are given by (22) and (20).

The conditions $M_{ijj} = 0$ relate the rest of the nonzero components of the moment tensor, M_{rrr} and $M_{r\theta\theta}$, as follows:

$$M_{rrr} + 2M_{r\theta\theta} = 0 \tag{26}$$

Furthermore, we find

$$M_{mr} = M_{rrr} - M'_{rrr} = 2M_{r\theta\theta} - M'_{rrr}, \tag{27}$$

where M_{mr} denotes the deviatoric part of the tensor $\boldsymbol{M}$ over its first two indices. This leads to $M_{\theta\theta r} = M'_{\theta\theta r}$. The formula (27) immediately gives

$$M_{r\theta\theta} = M'_{\theta\theta r} \tag{28}$$

Figure 3 illustrates the radial distribution of the equivalent and mean stresses obtained from the analytical solution in this paper. Along a radius of the hollow sphere matrix material, Σ_{eq} increases going outward while Σ_m shows the opposite behavior, which seems to confirm strong triaxaility effects in the vicinity of the inner surface of the hollow sphere structure, usually due to loading histories. There is a need to develop a full solution of the model problem (involving porosity effects) to confirm this trend.

4.3. ***Derivation of the velocity field.*** This section presents the analytical solution to the velocity field of the problem model presented. Following the procedure in [22] we use the results obtained for the stress invariants to rewrite the flow rule and so obtain a new differential equation for the velocity. Recall that $d_m = \frac{1}{3}\text{tr}(\boldsymbol{D}')$ and $d_{\text{eq}} = \frac{2}{3}(\boldsymbol{D}' : \boldsymbol{D}')^{2/3}$, where $\boldsymbol{D}'$ is the deviator of $\boldsymbol{D} = \frac{1}{2}\big(\nabla\mathcal{U} + (\nabla\mathcal{U})^t\big)$. Following Leblond's calculation [22, p. 97] we find

$$\frac{d_m}{d_{\text{eq}}} = \frac{\text{tr}(\boldsymbol{D}')}{2(\boldsymbol{D}' : \boldsymbol{D}')^{1/2}} = \frac{d\mathcal{U}/dr + 2\mathcal{U}/r}{2(\mathcal{U}/r - d\mathcal{U}/r)} = \frac{p}{2}\frac{\Sigma_0}{\Sigma_{\text{eq}}}\sinh\left(\frac{3}{2}\frac{\Sigma_m}{\Sigma_0}\right). \tag{29}$$

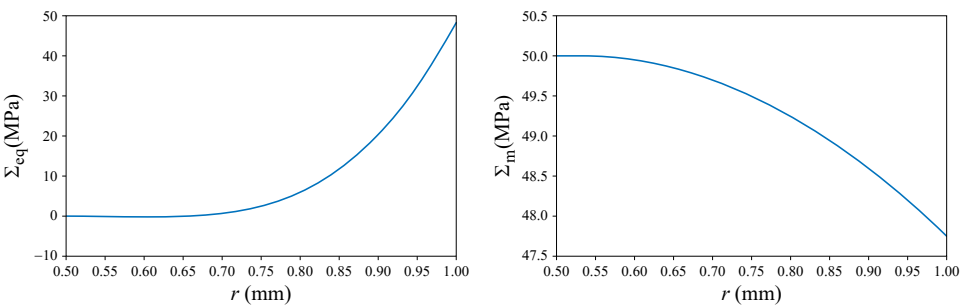

Figure 3. Radial distribution of equivalent stress Σ_{eq} (left) and mean stress Σ_m (right) for the Cauchy stress tensor.

Here the right-hand side is derived from the elimination of the plastic multiplier between the deviatoric and mean parts of the homogenized flow rule. Using the yield criterion we obtain for the right-hand side the value

$$\varphi(r) \equiv \frac{p}{2}\frac{\Sigma_0}{\Sigma_{\rm eq}}\sqrt{\frac{\Sigma_0^4}{4p^2}\left(p^2+1-\left(\frac{\Sigma_{\rm eq}^2}{\Sigma_0^2}+\frac{Q^2}{b^2\Sigma_0^2}\right)\right)}-1, \tag{30}$$

which involves both stress and moments. Thus the ordinary differential equation for the velocity is

$$\frac{d\mathcal{U}/dr+2\mathcal{U}/r}{2(\mathcal{U}/r-d\mathcal{U}/r)}=\varphi(r), \tag{31}$$

or yet

$$\frac{d\mathcal{U}}{dr}+g(r)\mathcal{U}=0, \quad \text{with} \quad g(r):=\frac{2}{r}\frac{1-\varphi(r)}{1+2\varphi(r)}. \tag{32}$$

Integrating by separation of variables yields

$$\mathcal{U}(r)=\lambda\exp\left(-\int_{r_0}^{r} g(\tau)\,d\tau\right), \tag{33}$$

where λ is a constant velocity determined from the boundary conditions.

4.4. ***The growth rate of the voids.*** The growth rate f of voids in the matrix satisfies

$$-\frac{d}{dt}\ln(1-f)=d_m=\frac{d\mathcal{U}}{dr}+\frac{2\mathcal{U}}{r}=\lambda\exp\left(-\int_{r_0}^{r}p(\tau)d\tau\right)\left(p(r)+\frac{2}{r}\right). \tag{34}$$

Solving for f gives

$$f=1-\exp\left(\int_{r_0}^{r}\xi(\gamma)d\gamma\right), \quad \text{with } \xi(\gamma)=\lambda\exp\left(-\int_{r_0}^{\gamma}g(\tau)d\tau\right)\left(g(\gamma)+\frac{2}{\gamma}\right).$$

The porous material's matrix contains small voids and a matrix that is incompressible; the dilatation $\mathrm{div}(\mathcal{U}(r)e_r)$ is associated to a growth $\dot{f}_2(r)$ of the porosity at the points located at a distance r of the central void, or equivalently to a growth of the mean radius, ρ, of the small cavities located at this position. Standard derivations based on incompressibility of the sound (void-free) matrix have demonstrated that the growth rate $\dot{\rho}/\rho$ of secondary voids is given by

$$\frac{\dot{\rho}}{\rho}=\frac{\dot{f}_2}{3f_2^0(1-f_2^0)}=\frac{\mathrm{div}(\mathcal{U}(r)e_r)}{f_2^0}=\frac{d_m}{f_2^0}. \tag{35}$$

When the porosity f_2^0 is small (which is the case for practical reasons), this becomes

$$\frac{\dot{\rho}}{\rho}=\frac{\dot{f}_2}{3f_2^0}=\frac{\dot{a}}{f_2^0}\exp\left(-\int_{r_0}^{r}g(\tau)d\tau\right)\left(g(r)+\frac{2}{r}\right). \tag{36}$$

In the vicinity of the large void where $r = a_0$, equation (36) reduces to

$$\frac{\dot{\rho}}{\rho}(r = a_0) = \frac{\dot{a}}{a_0}\left(f_2^0 p(a_0) + \frac{2}{f_2^0}\right). \tag{37}$$

Since the term in parentheses is close to $2/f_2^0$ when f_2^0 is very small, we see that the small voids near the boundary of the big one grow logarithmically faster than the larger void.

4.5. ***Discussion.*** We make some concluding remarks.

- When the characteristic length scale vanishes, all the components of the moment tensor also vanish by (19). This means that any second gradient effects in the GLPD model no longer exist. The yield criterion reduces to the original Gurson model yield criterion and the stress state of the material does not contain any length scale effects.
- Unlike [8], where porosity was disregarded, here we consider nonvanishing porosity, at the initial time where the porosity has not yet evolved. This will be sufficient to model ductile fracture mechanisms in metals with two populations of cavities. The study of porosity effects after the initial time is left for future investigations. (Perrin and Leblond [21; 22] have addressed these features, but the model their analysis is based on does not contain second gradient effects.)
- The boundary conditions $M_{rrr}(r = r_i, r_e) = 0$ ensure that the model does not account for boundary layer effects. Also, these boundary conditions induce no shear component effects.
- The expression of the void growth rate of the small voids in the matrix of the hollow sphere suggests that small voids located at the boundary of the large central void grow much more rapidly than the latter; this was first pointed out by Perrin and Leblond [21; 22] in the absence of nucleation, and is enhanced by nucleation as demonstrated in [8; 12]. As a consequence, the small voids may reach coalescence before the large central one. The presence of length scale effects in the growth rate will add microstructure effects on the fracture mechanisms pointed out above.

5. Conclusion

In this work we developed a solution for the micromorphic hollow sphere model under tension obeying the GLPD constitutive model when the porosity is constant at the initial time and we illustrate the analytic solutions provided previously by Enakousta's work when the porosity is neglected, but some effects of the strain gradient were involved. We express the stress solutions in terms of the invariants of the Cauchy stress tensor. The solution of the nonzero components of the moments due to the strain gradient effects are also provided in this work.The radial velocity

field and the growth rate of the small voids located in the matrix are derived; the expression of the latter suggest that small voids located near the larger one grow faster to form a shell of ruined material around the large void, a scenario that agrees very well with experimental observations. In addition, the solution developed in this work depends on the characteristic length scale and can be used as benchmark solution to assess micromorphic gradient models; the solution can also be used to test the efficiency of numerical implementation of gradient models into finite element software.

Appendix A: Constitutive relations of the GLPD model

A.1. ***Generalities.*** In the GLPD model, internal forces are represented through some ordinary second-rank symmetric Cauchy stress tensor $\boldsymbol{\Sigma}$ plus some additional third-rank "moment tensor" $\boldsymbol{M}$ symmetric in its first two indices only.[2] The components of $\boldsymbol{M}$ are related through the three conditions

$$M_{ijj} = 0, \tag{38}$$

which may be compared to the condition of plane stress in the theory of thin plates or shells. The virtual power of internal forces is given by

$$\mathcal{P}^{(i)} \equiv -\int_{\Omega} (\boldsymbol{\Sigma} : \boldsymbol{D} + \boldsymbol{M} \vdots \nabla \boldsymbol{D})\, d\Omega, \tag{39}$$

where Ω denotes the domain considered, $\boldsymbol{D} \equiv \frac{1}{2}\big(\nabla \boldsymbol{V} + (\nabla \boldsymbol{V})^{\mathrm{T}}\big)$ ($\boldsymbol{V}$ being the material velocity) the Eulerian strain rate, $\boldsymbol{\Sigma} : \boldsymbol{D} = \Sigma_{ij} D_{ij}$ is the double inner product and $\boldsymbol{M} \vdots \nabla \boldsymbol{D} \equiv M_{ijk} D_{ij,k}$ the triple inner product. The virtual power of external forces is given by

$$\mathcal{P}^{(e)} \equiv \int_{d\Omega} \boldsymbol{T}.\boldsymbol{V}\, dS, \tag{40}$$

where $\boldsymbol{T}$ represents some surface traction. The general equilibrium equations and boundary conditions corresponding to expressions (39) and (40) of the virtual powers of internal and external forces need not be given since they are not necessary for the numerical implementation.

The hypothesis of additivity of elastic and plastic strain rates reads

$$\boldsymbol{D} \equiv \boldsymbol{D}^e + \boldsymbol{D}^p, \quad \nabla \boldsymbol{D} \equiv (\nabla \boldsymbol{D})^e + (\nabla \boldsymbol{D})^p. \tag{41}$$

The elastic and plastic parts $(\nabla \boldsymbol{D})^e$, $(\nabla \boldsymbol{D})^p$ of the gradient of the strain rate here do *not* coincide in general with the gradients $\nabla(\boldsymbol{D}^e)$, $\nabla(\boldsymbol{D}^p)$ of the elastic and plastic parts of the strain rate.

[2] The component M_{ijk} is denoted $M_{k|ij}$ in [17]. The present notation leads to more natural-looking expressions.

A.2. ***Hypoelasticity law.*** The elastic parts of the strain rate and its gradient are related to the rates of the stress and moment tensors through the hypoelasticity law

$$\begin{aligned}\frac{d\Sigma_{ij}}{dt} &= \lambda\,\delta_{ij}D^e_{kk} + 2\mu D^e_{ij},\\ \frac{dM_{ijk}}{dt} &= \frac{b^2}{5}\big(\lambda\,\delta_{ij}(\nabla D)^e_{hhk} + 2\mu(\nabla D)^e_{ijk} - 2\lambda\,\delta_{ij}U^e_k - 2\mu(\delta_{ik}U^e_j + \delta_{jk}U^e_i)\big).\end{aligned} \tag{42}$$

Here λ and μ are the Lamé coefficients, b is the mean half-spacing between neighboring voids,[3] $d\Sigma_{ij}/dt$, dM_{ijk}/dt are the Jaumann (objective) time-derivatives of Σ_{ij}, M_{ijk}, given by

$$\begin{aligned}\frac{d\Sigma_{ij}}{dt} &\equiv \dot{\Sigma}_{ij} + \Omega_{ki}\Sigma_{kj} + \Omega_{kj}\Sigma_{ik},\\ \frac{dM_{ijk}}{dt} &\equiv \dot{M}_{ijk} + \Omega_{hi}M_{hjk} + \Omega_{hj}M_{ihk} + \Omega_{hk}M_{ijh},\end{aligned} \tag{43}$$

where $\boldsymbol{\Omega} \equiv \frac{1}{2}(\nabla \boldsymbol{V} - (\nabla \boldsymbol{V})^{\mathrm{T}})$ is the antisymmetric part of the velocity gradient, and finally $\boldsymbol{U}^e$ is a vector derived from (38), when written in rate form ($DM_{ijj}/Dt = 0$):

$$U^e_i = \frac{\lambda(\nabla D)^e_{hhi} + 2\mu(\nabla D)^e_{ihh}}{2\lambda + 8\mu}. \tag{44}$$

(This vector may be compared to the through-the-thickness component of the elastic strain rate in the theory of thin plates or shells, the value of which is fixed by the condition of plane stress).

A.3. ***Yield criterion.*** The plastic behavior is governed by the Gurson-like yield criterion

$$\frac{1}{\Sigma^2}\left(\Sigma^2_{\mathrm{eq}} + \frac{Q^2}{b^2}\right) + 2p\cosh\left(\frac{3}{2}\frac{\Sigma_m}{\Sigma}\right) - 1 - p^2 \le 0. \tag{45}$$

As before (pages 398 ff.), Σ_{eq} is the von Mises equivalent stress, Σ_m is the mean stress, b is the mean half-spacing between neighboring voids, Q^2 is given by (3), and Σ is an average yield stress in the heterogeneous metallic matrix (further discussed below). Finally, p is a parameter connected to the porosity f through the relation

$$p \equiv qf^*, \quad f^* \equiv \begin{cases} f & \text{if } f \le f_c,\\ f_c + \delta(f - f_c) & \text{if } f > f_c,\end{cases} \tag{46}$$

where q is *Tvergaard's parameter*, f_c the *critical porosity at the onset of coalescence of voids*, and $\delta > 1$ a factor describing the accelerated degradation of the material during coalescence [28; 29].

[3] In the homogenization procedure, b is the radius of the spherical elementary cell being considered.

A.4. ***Flow rule.*** The plastic parts of the strain rate and its gradient are given by the flow rule associated to the criterion (45) through normality (Φ is the yield function and η is the plastic multiplier; see page 398):

$$\begin{aligned} D^p_{ij} &= \eta \frac{d\Phi}{d\Sigma_{ij}}(\boldsymbol{\Sigma}, \boldsymbol{M}, \Sigma, f), \\ (\nabla D)^p_{ijk} &= \eta \frac{d\Phi}{dM_{ijk}}(\boldsymbol{\Sigma}, \boldsymbol{M}, \Sigma, f) + \delta_{ik} U^p_j + \delta_{jk} U^p_i, \end{aligned} \tag{47}$$

The terms $\delta_{ik} U^p_j + \delta_{jk} U^p_i$ in (47) represent a rigid-body motion of the elementary cell, left unspecified by the flow rule but fixed in practice by conditions (38). (The vector $\boldsymbol{U}^p$ may be compared to the through-the-thickness component of the plastic strain rate in the theory of thin plates or shells, the value of which is fixed by the condition of plane stress.)

The derivatives of the yield function in (47) are easily calculated to be

$$\begin{aligned} \frac{d\Phi}{d\Sigma_{ij}}(\boldsymbol{\Sigma}, \boldsymbol{M}, \Sigma, f) &= 3\frac{\Sigma'_{ij}}{\Sigma^2} + \frac{p}{\Sigma}\,\delta_{ij} \sinh\left(\frac{3}{2}\frac{\Sigma_m}{\Sigma}\right), \\ \frac{d\Phi}{dM_{ijk}}(\boldsymbol{\Sigma}, \boldsymbol{M}, \Sigma, f) &= \frac{1}{\Sigma^2 b^2}\left(\tfrac{2}{3} A_1 \delta_{ij} M_{mk} + 3A_2 M'_{ijk}\right). \end{aligned} \tag{48}$$

A.5. ***Evolution of internal parameters.*** The evolution of the porosity is governed by the classical equation resulting from approximate incompressibility of the metallic matrix:

$$\dot{f} = (1 - f)\,\mathrm{tr}\,\boldsymbol{D}^p. \tag{49}$$

The parameter Σ is given by

$$\Sigma \equiv \Sigma(E) \tag{50}$$

where $\Sigma(\epsilon)$ is the function which provides the yield stress of the matrix material in terms of the local equivalent cumulated plastic strain ϵ, and E represents some average value of this equivalent strain in the heterogeneous matrix. The evolution of E is governed by

$$(1 - f)\Sigma \dot{E} = \boldsymbol{\Sigma} : \boldsymbol{D}^p + \boldsymbol{M} \vdots (\nabla \boldsymbol{D})^p. \tag{51}$$

Appendix B: Balance equations and boundary conditions

To derive the equilibrium equations and boundary conditions presented in Section 2, we shall apply the principle of virtual work with a radial velocity $\boldsymbol{v}^\star \equiv v^\star_r e_r$, instead of departing from the global equilibrium equations and calculating $\nabla\nabla \boldsymbol{M}$

in spherical coordinates. The virtual power of internal forces is defined as

$$-\mathcal{P}^{(i)} \equiv 4\pi \int_{r_i}^{r_e} (\boldsymbol{\Sigma} : \boldsymbol{D}^\star + \boldsymbol{M} \vdots \nabla \boldsymbol{D}^\star)\, r^2 dr \tag{52}$$

Using the expressions of the strain and gradient of the strain, this becomes

$$\begin{aligned} -\mathcal{P}^{(i)} \equiv 4\pi \int_{r_i}^{r_e} \left(\Sigma_{rr} \frac{\partial v_r^\star}{\partial r} + 2\Sigma_{\theta\theta} \frac{v_r^\star}{r} + 2M_{\theta\theta r} \frac{\partial (v_r^\star / r)}{\partial r} \right) r^2 dr \\ + 4\pi \int_{r_i}^{r_e} \left(M_{\text{rrr}} \frac{\partial^2 v_r^\star}{\partial r^2} + M_{r\theta\theta} \left(\frac{1}{r} \frac{\partial v_r^\star}{\partial r} - \frac{v_r^\star}{r} \right) \right) r^2 dr. \end{aligned} \tag{53}$$

After integration by parts, this gives

$$\begin{aligned} -\mathcal{P}^{(i)} \equiv 4\pi \int_{r_i}^{r_e} \left(\frac{\partial (-r^2 \Sigma_{rr})}{\partial r} v_r^\star + 2r \Sigma_{\theta\theta} v_r^\star - 2 \frac{\partial (r^2 M_{\theta\theta r})}{\partial r} \frac{v_r^\star}{r} \right) dr \\ - 4\pi \int_{r_i}^{r_e} \left(\frac{\partial (r^2 M_{rrr})}{\partial r} \frac{\partial v_r^\star}{\partial r} + 4 v_r^\star \frac{\partial (r M_{r\theta\theta})}{\partial r} + v_r^\star M_{r\theta\theta} \right) dr \\ + 4\pi \left(r^2 \Sigma_{rr} v_r^\star + r^2 M_{rrr} \frac{\partial v_r^\star}{\partial r} + 2r M_{\theta\theta r} v_r^\star + 2r M_{r\theta\theta} v_r^\star \right) \Big|_{r_i}^{r_e}. \end{aligned} \tag{54}$$

Here as usual the notation $\Big|_{r_i}^{r_e}$ after a function of r represents the difference between its values at r_e and r_i. After development, this yields

$$\begin{aligned} -\mathcal{P}^{(i)} \equiv 4\pi \int_{r_i}^{r_e} \left(-2r \Sigma_{\text{rr}} - r^2 \frac{\partial \Sigma_{rr}}{\partial r} + 2r \Sigma_{\theta\theta} + r^2 \frac{\partial^2 M_{\text{rrr}}}{\partial r^2} + 4r \frac{\partial M_{rrr}}{\partial r} \right) v_r^\star \, dr \\ + 4\pi \int_{r_i}^{r_e} \left(-4M_{\theta\theta r} - 2r \frac{\partial M_{\theta\theta r}}{\partial r} - 8M_{r\theta\theta} - 4r \frac{\partial M_{r\theta\theta}}{\partial r} + 2M_{rrr} \right) v_r^\star dr \\ + 4\pi \left(\left(r^2 \Sigma_{rr} - \frac{\partial (r^2 M_{rrr})}{\partial r} + 2r M_{\theta\theta r} + 4r M_{r\theta\theta} \right) v_r^\star + r^2 M_{rrr} \frac{\partial v_r^\star}{\partial r} \right) \Big|_{r_i}^{r_e}. \end{aligned} \tag{55}$$

The application of the principle of virtual work (with the virtual power of external forces $\mathcal{P}^{(e)} = 4\pi b^2 T v_b^\star$, where T is a traction force applied on the outer surface of the hollow sphere) gives the balance equations

$$\begin{aligned} \frac{\partial \Sigma_{rr}}{\partial r} + \frac{2}{r}(\Sigma_{rr} - \Sigma_{\theta\theta}) - \frac{\partial^2 M_{rrr}}{\partial r^2} - \frac{4}{r} \frac{\partial M_{rrr}}{\partial r} - \frac{2}{r^2} M_{rrr} + \frac{2}{r^2} \frac{\partial M_{\theta\theta r}}{\partial r} \\ + \frac{4}{r^2} M_{\theta\theta r} + \frac{4}{r} \frac{\partial M_{r\theta\theta}}{\partial r} + \frac{8}{r^2} M_{r\theta\theta} = 0 \end{aligned} \tag{56}$$

and the boundary conditions

$$\begin{aligned} r^2 \Sigma_{rr} - \frac{\partial (r^2 M_{rrr})}{\partial r} + 2r M_{\theta\theta r} + 4r M_{r\theta\theta} = 0 \quad \text{for } r = r_i \text{ and } r = r_e, \\ M_{rrr} = 0 \quad \text{for } r = r_i \text{ and } r = r_e. \end{aligned}$$

References

[1] F. Ahad, K. Enakoutsa, K. Solanki, and D. Bammann, "Nonlocal modeling in high velocity impact failure of aluminum 6160-T6", *Int. J. Plast.* **55** (2013), 108–132.

[2] G. A.L., "Continuum theory of ductile rupture by void nucleation and growth, I: Yield criteria and flow rules for porous ductile media", *ASME J. Engng. Mater. Technol.* **99** (1977), 2–15.

[3] U. Andreaus, F. dell'Isola, I. Giorgio, L. Placidi, T. Lekszycki, and N. L. Rizzi, "Numerical simulations of classical problems in two-dimensional (non) linear second gradient elasticity", *Internat. J. Engrg. Sci.* **108** (2016), 34–50.

[4] J.-M. Bergheau, J.-B. Leblond, and G. Perrin, "A new numerical implementation of a second-gradient model for plastic porous solids, with an application to the simulation of ductile rupture tests", *Comput. Methods Appl. Mech. Engrg.* **268** (2014), 105–125.

[5] R. Burson and K. Enakoutsa, "Closed-form analytic solutions of the problem of a hollow sphere made of second gradient plastic porous material and subjected to hydrostatic loading", pp. 37–67 in *Theoretical analyses, computations, and experiments of multiscale materials: a tribute to Francesco dell'Isola*, edited by I. Giorgio et al., Adv. Struct. Mater. **175**, Springer, 2022.

[6] F. dell'Isola, A. Della Corte, and I. Giorgio, "Higher-gradient continua: the legacy of Piola, Mindlin, Sedov and Toupin and some future research perspectives", *Math. Mech. Solids* **22**:4 (2017), 852–872.

[7] K. Enakoutsa, *Modèle non-locaux en rupture ductile des métaux*, Ph.D. thesis, Université Pierre et Marie Curie (Paris VI), 2007.

[8] K. Enakoutsa, "Exact results for the problem of a hollow sphere subjected to hydrostatic tension and made of micromorphic plastic porous materials", *Mech. Res. Commun.* **49** (2013), 1–7.

[9] K. Enakoutsa, "Some new applications of the GLPD micromorphic model of ductile fracture", *Math. Mech. Solids* **19**:3 (2014), 242–259.

[10] K. Enakoutsa, "An analytic benchmark solution to the problem of a generalized plane strain hollow cylinder made of micromorphic plastic porous metal and subjected to axisymmetric loading conditions", *Math. Mech. Solids* **20**:9 (2015), 1013–1025.

[11] K. Enakoutsa and J. B. Leblond, "Numerical implementation and assessment of the GLPD micromorphic model of ductile rupture", *Eur. J. Mech. A/Solids* **28** (2009), 445–460.

[12] K. Enakoutsa, J.-B. Leblond, and B. Audoly, "Influence of continuous nucleation of secondary voids upon growth and coalescence of cavities in porous ductile metals", in *Proceedings of the* 11*th international conference on fracture* (Turin, Italy), edited by A. Carpinteri, 2005.

[13] K. Enakoutsa, J. B. Leblond, and G. Perrin, "Numerical implementation and assessment of a phenomenological nonlocal model of ductile rupture", *Comput. Meth. Appl. Mech. Engng.* **196** (2007), 1946–1957.

[14] K. Enakoutsa, K. Solanki, F. Ahad, Y. Tjiptowidjojo, and D. Bammann, "Damage smoothing effects in a delocalized rate sensitivity model for metals", *Theoret. Appl. Mech. Lett.* **2**:5 (2012), art. id. 5–051005.

[15] K. Enakoutsa, K. Solanki, F. Ahad, Y. Tjiptowidjojo, and D. Bammann, "Using damage delocalization to model localization phenomena in Bammann–Chiesa–Johnson metals", *J. Eng. Mater. Tech.* **134**:4 (2012), art. id. 041014.

[16] I. Giorgio, U. Andreaus, F. dell'Isola, and T. Lekszycki, "Viscous second gradient porous materials for bones reconstructed with bio-resorbable grafts", *Extreme Mech. Lett.* **13** (2017), 141–147.

[17] M. Gologanu, J. B. Leblond, G. Perrin, and J. Devaux, "Recent extensions of Gurson's model for porous ductile metals", pp. 61–130 in *Continuum micromechanics*, edited by P. Suquet, CISM Courses and Lectures **377**, Springer, 1997.

[18] A. L. Gurson, "Continuum theory of ductile rupture by void nucleation and growth, I: Yield criteria and flow rules for porous ductile media", *J. Engrg. Mater. Technol.* **99**:1 (1977), 2–15.

[19] J. Leblond, G. Perrin, and J. Devaux, "Bifurcation effects in ductile metals with nonlocal damage", *ASME J. Applied . Mech.* **61** (1994), 236–242.

[20] K. Nahshon and J. Hutchinson, "Modification of the Gurson model for shear failure", *Eur. J. Mech. A/Solids* **27** (2008), 1–17.

[21] G. Perrin and J.-B. Leblond, "Analytical study of a hollow sphere made of plastic porous material and subjected to hydrostatic tension Application to some problems in ductile fracture of metals", *Int. J. Plast.* **6** (1990), art. id. 677699.

[22] G. Perrin and J.-B. Leblond, "Accelerated void growth in porous ductile solids containing two populations of cavities", *Int. J. Plast.* **16** (2000), art. id. 91v120.

[23] G. Pijaudier-Cabot and Z. Bazant, "Nonlocal damage theory", *ASCE J. Engrg. Mech.* **113** (1987), 1512–1533.

[24] L. Placidi, E. Barchiesi, A. Misra, and D. Timofeev, "Micromechanics-based elasto-plastic-damage energy formulation for strain gradient solids with granular microstructure", *Contin. Mech. Thermodyn.* **33**:5 (2021), 2213–2241.

[25] J. C. Reiher, I. Giorgio, and A. Bertram, "Finite-element analysis of polyhedra under point and line forces in second-strain gradient elasticity", *J. Engrg. Mech.* **143**:2 (2017), art. id. 04016112.

[26] J. R. Rice and D. M. Tracey, "On the ductile enlargement of voids in triaxial growth holes", *J. Mech. Phys. Solids* **17** (1969), 210–217.

[27] D. Scerrato, A. M. Bersani, and I. Giorgio, "Bio-inspired design of a porous resorbable scaffold for bone reconstruction: a preliminary study", *Biomimetics* **6**:1 (2021), art. id. 18.

[28] V. Tvergaard, "Influence of voids on shear band instabilities under plane strain conditions", *Int. J. Fracture* **17** (1981), 389–407.

[29] V. Tvergaard and A. Needleman, "Analysis of cup-cone fracture in a round tensile bar", *Acta Metall.* **32** (1984), 157–169.

[30] V. Tvergaard and A. Needleman, "Effects of nonlocal damage in porous plastic solids", *Int. J. Solids Struct.* **32** (1995), 1063–1077.

[31] V. Tvergaard and A. Needleman, "Nonlocal effects on localization in a void-sheet", *Int. J. Solids Struct.* **34** (1997), 2221–2238.

Received 20 May 2022. Revised 11 Sep 2022. Accepted 7 Nov 2022.

ROY BURSON: roy.burson.618@my.csun.edu
Department of Mathematics, California State University, Northridge, CA, United States

KOFFI ENAKOUTSA: koffi@math.ucla.edu
Department of Mathematics, California State University, Northridge, CA, United States

and

Department of Mathematics, University of California Los Angeles, Los Angeles, CA, United States

MATHEMATICS AND MECHANICS OF COMPLEX SYSTEMS

msp.org/memocs

MEMOCS is a journal of the International Research Center for the Mathematics and Mechanics of Complex Systems at the Università dell'Aquila, Italy.

See inside back cover or msp.org/memocs for submission instructions.

The subscription price for 2022 is US $195/year for the electronic version, and $255/year (+$25, if shipping outside the US) for print and electronic. Subscriptions, requests for back issues and changes of subscriber address should be sent to MSP.

Mathematics and Mechanics of Complex Systems (ISSN 2325-3444 electronic, 2326-7186 printed) at Mathematical Sciences Publishers, 798 Evans Hall #3840, c/o University of California, Berkeley, CA 94720-3840 is published continuously online.

MEMOCS peer review and production are managed by EditFlow® from MSP.

PUBLISHED BY

mathematical sciences publishers

nonprofit scientific publishing

http://msp.org/

Mathematics and Mechanics of Complex Systems
vol. 10 no. 4 2022

MEMOCS is a journal of the International Research Center for the Mathematics and Mechanics of Complex Systems at the Università dell'Aquila, Italy.